

# Shear failure of plain concrete in strain localized area

Y. Kaneko & H. Mihashi

*Tohoku University, Sendai, Miyagi, Japan*

S. Ishihara

*Asanuma Corporation, Takatsuki, Osaka, Japan*

**ABSTRACT:** The objective of this paper is to study the shear failure of plain concrete in strain localized area. An experimental study on plain concrete subjected to shear was carried out. The shape of specimen was a horizontally double-notched concrete block. In order to study the shear softening characteristics of plain concrete, a mechanical model for the macroscopic shear failure is applied to the experiments, focusing on the entire load-displacement relation. The method makes use of rotating smeared crack concept and truss model, combined in a simple model. The analysis employs the development of multiple diagonal cracks and macroscopic fictitious shear crack propagation. The model is found in good agreement with the experiments. The analytical results point out that the shear softening characteristics depend on the size of strain localized area.

**Keywords:** Direct shear test, Shear softening, Fictitious shear crack, Strain localization

## 1 INTRODUCTION

The research on cracking behavior of concrete has been largely progressed after the proposal of Fictitious Crack Model (FCM) by Hillerborg et al. (1976). The model describes the mode I fracture behavior at the cracking process zone by means of tension softening curve, which is the function of tensile strength and fracture energy. The tension softening curve is the relation between the cohesive force along the fictitious crack and the crack width. After this proposal, many experimental and analytical research works on mode I fracture of concrete have been carried out and it becomes possible to obtain experimentally the fracture parameter such as fracture energy and tension softening curve.

It has been known that the actual fracture mode observed in concrete structures is complex behavior associated with structural system, loading and boundary conditions and so on. Therefore, it is necessary to comprehend the physical behavior on mixed mode fracture combined with mode I and II, to develop the mechanical model to describe the behavior, and to obtain the mechanical parameters to express quantitatively the model based on the

standard test. However, most of evaluation methods on shear fracture behavior of concrete structures are based on experiments, and the theoretical approach such as a limit analysis does not give the sufficient solution regarding deformation behavior. In addition, there are a few researches on shear softening characteristics and the generalized definition on shear softening is not confirmed.

For this technical background, the objective of this research is to expand the concept of so-called fictitious crack model to mode II shear fracture, to develop a mechanical model and to propose finally a simple test method with which the necessary mechanical parameters are identified for modeling.

Authors have constructed the shear fracture sequence based on the fracture process observed in the experiments of a direct shear test, developed a mechanical model and identified the correlation between shear softening behavior and aggregate interaction behavior (Kaneko et al. 2001). The methodology of this mechanical model has been applied to the shear-off failure of plain and fiber reinforced concrete shear key joints (Kaneko et al. 1993ab, Kaneko 1993) and the shear failure of reinforced concrete membrane elements (Kaneko

1998) in which the force-displacement characteristics were predicted appropriately.

Based on the research achievement, a mechanical model is applied to the direct shear test (Ishihara et al. 2003) focusing on the entire deformation behavior of concrete in this paper.

## 2 EXPERIMENTAL WORK

As shown in Figure 1, the direct shear test was conducted with the parameters of the notch-distance and with joint or without joint to obtain the post-peak characteristics and the deformation behavior at the localized shear failure area. In the test, the ratio of notch-distance ( $a$ ) to the specimen-height ( $D$ ) was set as 0.1 or 0.17, and the fracture behavior at the shear failure area was observed by means of a microscope.

In the specimens, the horizontal wedge-type notch with the maximum opening displacement of 5 mm was installed at upper and lower positions, and two types of specimens were adopted such as the notch distance of 60 mm ( $a/D=0.1$ , UJ60 and JR60 series) and 100mm ( $a/D=0.17$ , UJ100 series). Here, UJ stands for the unjointed specimens and JR for the jointed ones with surface roughness of 2.0 mm.

The compressive strength  $f'_c$  and splitting tensile strength  $f_t$  of concrete obtained with the same mixing proportion are summarized as follows: concrete C01 ( $f'_c=30.4\text{MPa}$ ,  $f_t=2.47\text{MPa}$ ) for UJ series; concrete C01 and concrete C02 ( $f'_c=35.5\text{MPa}$  and  $f_t=3.0\text{MPa}$ ) for JR series. The maximum aggregate size was 15 mm for relatively narrow notch-distance. The basic support (loading point) condition was the pin-support at the upper and the fixed one at the lower. The specimens of UJ60-8 and 9 were supported at both pin-supports. In UJ60 series, the vertical and horizontal displacements between A1-bolt and A2-bolt were measured at both frontage and reverse, as shown in Figure 1.

Regarding the fracture behavior, the following phenomena were observed. In the specimens of UJ60-1, 2 and 3, the flexural cracks initiated at both upper and lower notches. Each flexural crack propagated to the opposite notch tip and finally reached to it. In the specimens of UJ60-4, 5, 6 and 7, only one flexural crack initiated and reached to the opposite notch tip. On the other hand, in the specimens of UJ60-8 and 9, the flexural cracks first initiated and propagated similar to the specimens of UJ60-1, 2 and 3. Subsequently, the shear cracks were observed near the center of shear plane

between both notches with the microscope. Specifically, in the specimen of UJ60-8, the shear cracks dominated the failure mechanism and the compression struts between both notches finally crushed as shown in Figure 2. In the specimen of UJ60-9, the shear cracks stopped propagating and a flexural crack propagated to the opposite notch tip and finally reached to it.

In the specimens of UJ100-1 and 2, only one flexural crack first initiated and propagated to the opposite notch tip. Subsequently, the shear cracks were observed at the shear plane between both notches with the microscope. Finally, the shear cracks dominated the failure mechanism and the compression struts between both notches crushed. In the specimens of UJ100-3, the similar behavior was observed to the specimens of UJ100-1 and 2. However, the final failure was caused by not shear cracks between both notches but flexural cracks that reached the notch tip.

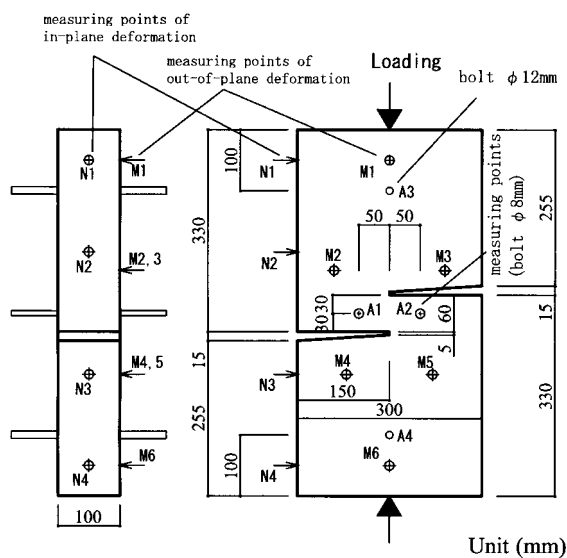


Figure 1. Specimens and Loading System of UJ 60 (Frontage)

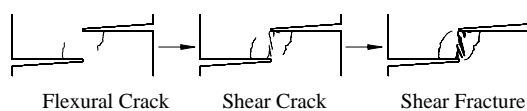


Figure 2. Cracking Patterns of Specimen UJ60-8 (Frontage)

### 3 SHEAR FRACTURE MODEL

#### 3.1 Modeling for Strain Localized Area

The damage area (width:  $W_{da}$ ) associated with shear failure is modeled by a single fictitious macroscopic shear crack as shown Figure 3(a) and (b). The cracking behavior is modeled based on the fracture sequence defined in the previous research (e.g., Kaneko et al. 2001). The following simple fracture sequence of diagonal multiple crack is macroscopically constructed and is schematically shown in Figure 3(c).

1. At the damaged area, diagonal multiple cracks initiate along the principal stress axis, and finally the shear fracture zone is formulated as distributed cracks. The diagonal multiple cracks are assumed evenly distributed along the shear-fractured zone with a certain angle of inclination.
2. With further shear loading, the diagonal multiple cracks are assumed to rotate following the principal stress axis under mode I condition.
3. The tensile strain of cracks and the compressive strain of struts between each crack and the next increase continuously, and the macroscopic shear softening starts associated with the crushing failure of compression struts. Specifically, diagonal multiple cracks are coalesced into the macroscopic fictitious shear crack caused by the highly localized strain distribution.

In order to evaluate a quantity of energy, the strain at the damaged area is translated to both the shear slip displacement and the shear crack opening displacement of macroscopic fictitious shear crack. In the present approach, the fracture process of diagonal multiple cracks is modeled by means of a combination of a rotating smeared crack concept

and a truss model. The intent of this approach is based on the fact that it is often desirable to find general analytical solutions, which are much easier to handle than numerical solutions produced by nonlinear FEM analysis.

#### 3.2 Rotating Smeared Crack Model

The present mechanical model satisfies three basic requirements: equilibrium, compatibility and material constitutive laws. Stress transformation conditions (equilibrium) in a cracked element at the damaged area are formulated based on the works of Vecchio & Collins (1986) and Hsu et al. (1987).

In this modeling, stress and strain are assumed uniformly distributed as averaged ones over the entire damaged area. After diagonal cracking occurs, a series of diagonal compression struts is formed in the compression direction (c-direction). The element takes only compressive stress  $\sigma_c$  in the c-direction of compression struts and only tensile stress  $\sigma_t$  in the tension direction (t-direction) transverse to compression struts. Shear stress  $\tau_{ct}$  along the cracked element is assumed zero. Thus,  $\sigma_c$  and  $\sigma_t$  are always principal stresses of this system. The angle between the x-y and c-t coordinate systems is designated as  $\theta$  as shown in Figure 4. This angle is also the angle of inclination of compression struts with respect to the x-axis. The averaged stresses and strains of concrete element in the two coordinate systems, x-y and c-t, are transformed according to the following equations.

$$\sigma_x = \sigma_c \cos^2 \theta + \sigma_t \sin^2 \theta \quad (1a)$$

$$\sigma_y = \sigma_c \sin^2 \theta + \sigma_t \cos^2 \theta \quad (1b)$$

$$\tau_{xy} = (\sigma_c - \sigma_t) \sin \theta \cos \theta \quad (1c)$$

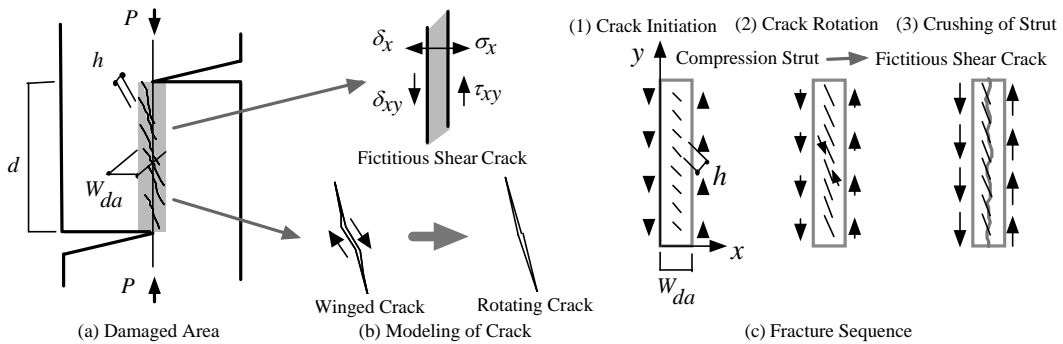


Figure 3. Modeling for Shear Fracture at Damaged Area

$$\varepsilon_x = \varepsilon_c \cos^2 \theta + \varepsilon_t \sin^2 \theta \quad (1d)$$

$$\varepsilon_y = \varepsilon_c \sin^2 \theta + \varepsilon_t \cos^2 \theta \quad (1e)$$

$$\gamma_{xy} = 2(\varepsilon_c - \varepsilon_t) \sin \theta \cos \theta \quad (1f)$$

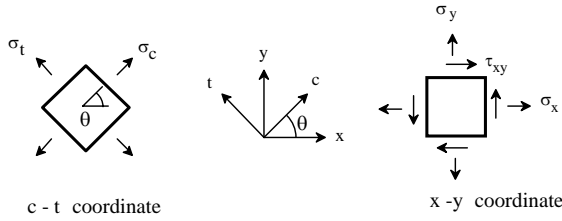


Figure 4. Stress Transformation System

For the concrete element between the uniformly distributed diagonal cracks, which rotate along the principal stress axis, the following constitutive laws are applied.

The assumed tensile stress-strain relation of plain concrete in the direction perpendicular to the compression struts is formulated by the following equations. The bilinear tensile stress-deformation relation originally proposed by Hillerborg (1985) as a tension softening concept is adopted for the descending branch based on the crack band theory (Bazant and Oh 1983) as shown in Figure 5(a).

$$\sigma_t = E_c \varepsilon_t \quad : \varepsilon_t \leq \varepsilon_{cr} \quad (2a)$$

$$\sigma_t = f_t \frac{\left( \varepsilon_{m1} - \frac{\varepsilon_{cr}}{3} - \frac{2\varepsilon_t}{3} \right)}{(\varepsilon_{m1} - \varepsilon_{cr})} \quad : \varepsilon_{cr} < \varepsilon_t \leq \varepsilon_{m1} \quad (2b)$$

$$\sigma_t = \frac{f_t (\varepsilon_{m2} - \varepsilon_t)}{3(\varepsilon_{m2} - \varepsilon_{m1})} \quad : \varepsilon_{m1} < \varepsilon_t \leq \varepsilon_{m2} \quad (2c)$$

$$\varepsilon_{cr} = \frac{f_t}{E_c} \quad (2d)$$

$$\varepsilon_{m1} = \varepsilon_{cr} + \frac{4G_F}{5f_t h} \quad (2e)$$

$$\varepsilon_{m2} = \varepsilon_{cr} + \frac{18G_F}{5f_t h} \quad (2f)$$

$$h = \frac{W_{da}}{5} \quad (2g)$$

where  $E_c$  = Young's modulus;  $f_t$  = tensile strength of concrete;  $\varepsilon_{cr}$  = cracking strain;  $\varepsilon_{m1}$  and  $\varepsilon_{m2}$  = post-cracking characteristic strains; and  $G_F$  = fracture energy.  $h$  is the interval between each diagonal crack and the next as shown in Figure 3 (Kaneko et al. 2001).

The assumed compressive stress-strain relation in the direction of compression struts is constructed based on the works of Soroushian et al. (1986) and Hognestad (1951) as shown in Figure 5(b). In addition, softening of concrete struts related to tensile strain in the direction perpendicular to struts is considered based on the work of Vecchio & Collins (1986). Thus, assumed stress-strain relations are described by the following equations (Kaneko et al. 2001).

$$\sigma_c = \frac{f'_c}{\lambda} \left[ \frac{2\varepsilon_c}{\varepsilon_{c0}} - \left( \frac{\varepsilon_c}{\varepsilon_{c0}} \right)^2 \right] \quad : \varepsilon_c \leq \varepsilon_{c0} \quad (3a)$$

$$\sigma_c = \frac{f'_c}{\lambda} [1 - Z(\varepsilon_c - \varepsilon_{c0})] \quad : \varepsilon_{c0} < \varepsilon_c \leq \varepsilon_{cu1} \quad (3b)$$

$$\sigma_c = \frac{0.2f'_c}{\lambda} \quad : \varepsilon_{cu1} < \varepsilon_c \quad (3c)$$

$$\lambda = 0.8 + 0.34 \frac{\varepsilon_t}{\varepsilon_{c0}} \geq 1.0 \quad (3d)$$

$$\varepsilon_{c0} = \frac{2f'_c}{E_c} \quad (3e)$$

$$\varepsilon_{cu1} = \frac{0.8}{Z} + \varepsilon_{c0} \quad (3f)$$

$$Z = \frac{0.5}{\frac{3 + 145\varepsilon_{c0}f'_c}{145f'_c - 1000} - \varepsilon_{c0}} \quad (3g)$$

where  $f'_c$  = compressive strength;  $\varepsilon_{c0}$  = associated strain; and  $\lambda$  = coefficient to take care of the softening phenomena.

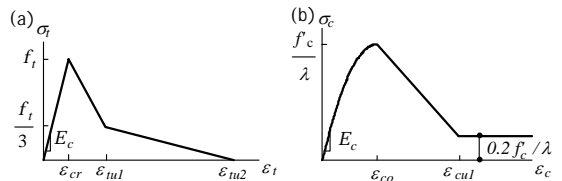


Figure 5. Stress-strain Relationship (a)Tension; (b)Compression

Young's modulus of concrete was estimated by the following relation (Chen 1982, Kaneko et al.

2001). The fracture energy was estimated as 0.1 N/mm, a value often used by many researchers (e.g., Rots & Blaauwendraad 1989, Balakrishnan & Murray 1988).

$$E_c = \frac{4733\sqrt{f'_c}}{0.82} + 1.8776 \quad (4)$$

In the present modeling, a principal strain ratio  $\nu_a$  ( $=\varepsilon_c/\varepsilon_t$ , or apparent Poisson's ratio) is constructed to evaluate simply a complex fracture sequence governed by a tensile strain. It is assumed that the relation between the tensile strain and compressive strain of a compression strut are related by the ratio  $\nu_a$  defined as:

$$\nu_a = \varepsilon_c / \varepsilon_t = 0.2 \quad : \varepsilon_c \leq \varepsilon_0 \quad (5a)$$

$$\nu_a = 0.5 \quad : \varepsilon_{c0} < \varepsilon_c \quad (\text{model 1}) \quad (5b)$$

$$\nu_a = 0.2 \quad : \varepsilon_{c0} < \varepsilon_c \quad (\text{model 2}) \quad (5c)$$

The ratio  $\nu_a$  is a salient feature in the present mechanical model and is defined as  $\varepsilon_c/\varepsilon_t$  for the case in which the tensile strain controls the deformation of the structure. This is because the coalescence of diagonal cracks could be achieved by high strain localization between each diagonal crack and the next. The aim of this model is to eliminate a numerical iteration in the calculation of the stress and strain in both tension and compression (see the detail in Kaneko et al. 1993ab, Kaneko et al. 2001). Specifically, the compressive strain ( $\varepsilon_c$ ) is calculated by Equation (5) for monotonically increasing tensile strain ( $\varepsilon_t$ ). The tensile and compressive stresses can be then calculated by substituting the known values of tensile and compressive strain into each constitutive model without numerical iteration.

The ratio  $\nu_a$  was formulated based on structural experiments (Vecchio & Collins 1986, Mansure & Ong 1991). The model 1 gives a mean value of scattered experimental data and the model 2 is defined as a constant value of  $\nu_a$  without steep increase of compressive strain. In the analysis for deep beams (Kaneko & Mihashi 2002), the model 2 gave stable converged solutions associated with the steep drop after the maximum load. Therefore, in this paper, the model 2 is adopted to study the post-peak characteristics.

The load  $P$ , the shear sliding displacement ( $\delta_{xy}$ ) and the crack opening displacement ( $\delta_x$ ) orthogonal to shear plane at the macroscopic fictitious shear crack are calculated for the specimens with the width ( $b$ ) by the following equations.

$$P = \tau_{xy} bd \quad (6a)$$

$$\delta_{xy} = \gamma_{xy} W_{da} \quad (6b)$$

$$\delta_x = \varepsilon_x W_{da} \quad (6c)$$

Using the principal strain ratio ( $\nu_a = \varepsilon_c/\varepsilon_t$ ) and the specified confined stress ( $\sigma_x = 0.0$ ), the preceding 11 unknowns ( $\sigma_x, \sigma_y, \tau_{xy}, \varepsilon_x, \varepsilon_y, \gamma_{xy}, \sigma_t, \sigma_c, \varepsilon_t, \varepsilon_c$ , and  $\theta$ ) are reduced to 9. By selecting one of them ( $\varepsilon_t$ ) as a known value, the remaining 8 unknowns can be obtained from a set of 8 equilibrium, compatibility and constitutive equations. Hence, one can develop the relation between the average shear stress  $\tau_{xy}$  and the average shear strain  $\gamma_{xy}$  by the following steps:

- a) Select a value of  $\varepsilon_t$ ;
- b) Assume  $\nu_a = 0.2$  (model 2);
- c) Calculate  $\varepsilon_c$  from  $\nu_a = \varepsilon_c/\varepsilon_t$ ;
- d) Calculate  $\sigma_t, \sigma_c$  and  $\lambda$  from Equations (2) and (3);
- e) Calculate  $\theta$  from Equation (1a) with specified  $\sigma_x (= 0.0)$ ;
- f) Calculate  $\tau_{xy}, \gamma_{xy}$  and  $\varepsilon_x$  from Equation (1);
- g) Calculate the parameters associated with load and displacement from Equation (6).

## 4 VERIFICATION STUDY

### 4.1 Load-displacement relation

The applicability of the mechanical model is mainly examined with three unjointed specimens of UJ60-8, UJ100-1 and UJ100-2, which showed obvious shear failure between two notches. Figure 6(a) shows the comparison of load-displacement relation between experiment and analysis. In the analysis, the damaged area width ( $W_{da}$ ) of 15 mm observed in the experiment of UJ60-8 was adopted. It is realized that the prediction is in relatively good agreement with the experimental results for the entire range of loading consisting of the post-peak region. Specifically, in the specimen of UJ60-8, the stiffness in the experiment reduces around the loading level of 20 kN. This is caused by the flexural cracks near the notch tip, which is not considered in the mechanical model.

In the specimen of UJ100-2, good agreement between the experiment and the analysis is observed, except that the experimental result keeps the loading level awhile after the peak load. This is

caused by the rotation of specimen due to the one-sided flexural crack. Figures 6(b) and (c) show the comparison of load-displacement relation between the experiment and the analysis employing several widths ( $W_{da}$ ) of damaged area. It is clear that the larger width ( $W_{da}$ ) gives the larger post-peak ductility with a slight reduction of the peak load.

Figure 6(d) shows the comparison of load-displacement relation between the experiment for jointed specimens and the analysis employing  $W_{da}=15\text{mm}$  and the lower value of  $f'_c$  in the jointed specimens (concrete C01). The predictions are in good agreement with the experimental results as well as the analyses for unjointed specimens, except the specimen of JR60-1, which gave extremely low peak load. It was observed that the cracking sequence of JR60-1 deviated from the

joint-plane, which was completely different from the other jointed specimens. Thus, it is clarified that there exists the strain localized area even in the jointed specimens with sufficiently roughened surface as well as unjointed specimens of UJ60-8, UJ100-1 and UJ100-2.

Figure 7(a) shows the comparison of shear softening characteristics and dissipated energy at the damaged area employing several widths ( $W_{da}$ ) of damaged area. The dissipated energy is defined here as the area under the shear stress-shear displacement curve up to the considered shear displacement. It is clear that the larger width ( $W_{da}$ ) gives the larger post-peak ductility and larger dissipated energy with a slight reduction of the peak stress.

Figure 7(b) shows the stress-tensile strain curves

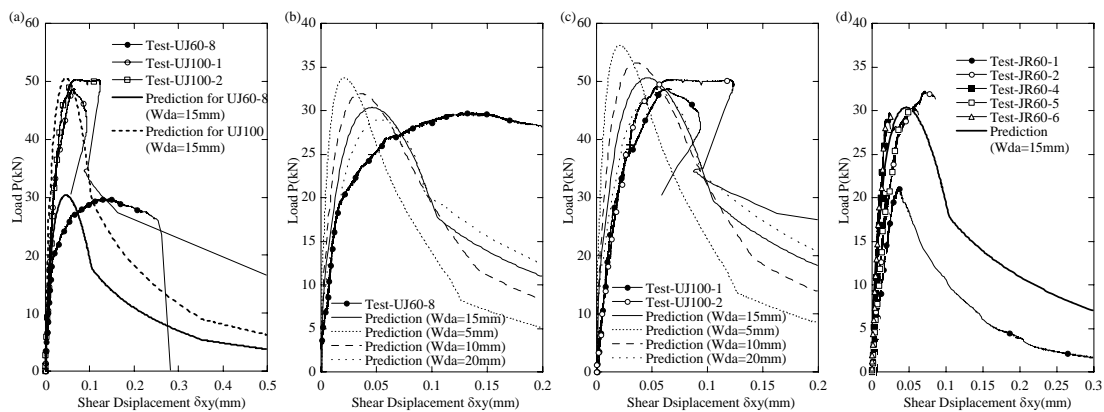


Figure 6. Comparison of Load-Displacement Curves between Experiment and Analysis

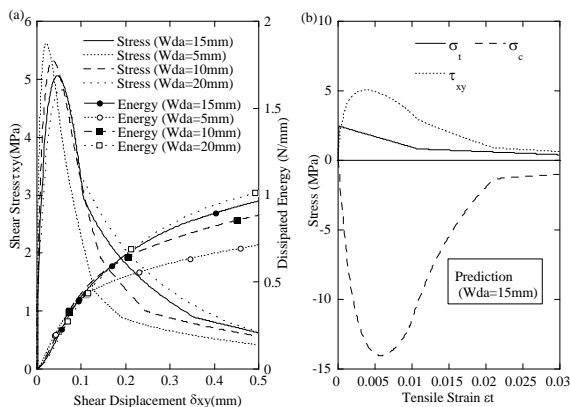


Figure 7. Shear Softening Characteristics and Constitutive Laws

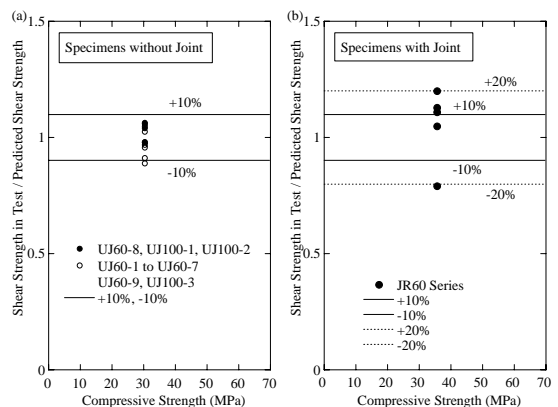


Figure 8. Comparison of Shear Strength

obtained in the analysis. It is realized that the compressive stress  $\sigma_c$  in a compression strut becomes highly close to the peak stress and the stress point in the tensile constitutive law is on the first softening region when the shear stress  $\tau_{xy}$  reaches the peak stress. This numerical phenomenon is considered in the formulation of shear strength in the next section.

#### 4.2 Formula for Shear Strength

In order to verify the proposed mechanical model alternatively, the formula for the shear strength is developed based on the assumption: the compressive stress  $\sigma_c$  in a compression strut becomes equal to the peak and the stress point in the tensile constitutive law is on the first softening region when the shear stress  $\tau_{xy}$  reaches the peak stress (see Figure 7(b)). Here, the values of  $\sigma_c, f'_c, \varepsilon_c, \varepsilon_{c0}$  are considered negative since the tensile stress and strain are defined positive and the compressive stress and strain are negative.

Substituting Equations (5a) and (3d) with  $x = -\varepsilon_t/\varepsilon_{c0}$  ( $>0$ ) into Equation (3a), one can obtain the following equation.

$$0.8\sigma_c + 0.34\sigma_c x - 0.4f'_c x + 0.04f'_c x^2 = 0.0 \quad (7)$$

The conditions for  $x$  to give the maximum (local minimum) of  $\sigma_c$  are as follows:

$$\frac{d\sigma_c}{dx} = 0.0, \quad \frac{d^2\sigma_c}{dx^2} > 0.0 \quad (8a,8b)$$

Differentiate Equation (7) with respect to  $x$ , one can obtain the following equations.

$$0.8\frac{d\sigma_c}{dx} + 0.34\sigma_c + 0.34x \frac{d\sigma_c}{dx} - 0.4f'_c + 0.08f'_c x = 0.0 \quad (9)$$

$$0.8\frac{d^2\sigma_c}{dx^2} + 2 \times 0.34\frac{d\sigma_c}{dx} + 0.34x \frac{d^2\sigma_c}{dx^2} + 0.08f'_c = 0.0 \quad (10)$$

Substituting Equations (7) and (8a) into Equation (9), one can obtain the following equation.

$$0.0136f'_c x^2 + 0.064f'_c x - 0.32f'_c = 0.0 \quad (11)$$

Then,  $x$  ( $=x^{cr}$ ) associated with the maximum (local minimum) of  $\sigma_c$  is calculated as follows:

$$x^{cr} = -\frac{\varepsilon_t^{cr}}{\varepsilon_{c0}} = 3.0383 \approx 3.0 \quad (12)$$

Substituting Equation (12) into Equation (10), one can see that the condition with Equation (8b) is satisfied as follows:

$$\frac{d^2\sigma_c}{dx^2} = -\frac{0.08f'_c}{0.8 + 0.34 \times 3.0} > 0.0 \quad (13)$$

Substituting Equation (12) into Equation (7), one can obtain the maximum (local minimum) of  $\sigma_c$  as follows:

$$\sigma_c^{max} = 0.462f'_c \quad (14)$$

Substituting Equations (3e) and (12) into Equation (2b), one can obtain the tensile stress  $\sigma_t$  ( $=\sigma_t^{cr}$ ) associated with  $\sigma_c^{max}$  as follows:

$$\sigma_t^{cr} = f_t + \frac{5hf_t^2}{6E_c G_f} (f_t + 6f'_c) \quad (15)$$

Substituting the condition of  $\sigma_x=0.0$  into Equation (1a), one can obtain  $\theta$  ( $=\theta^{cr}$ ) associated with  $\sigma_c^{max}$  as follows:

$$\theta^{cr} = \cos^{-1} \sqrt{\frac{\sigma_t^{cr}}{\sigma_t^{cr} - \sigma_c^{max}}} \quad (16)$$

Substituting Equations (14)-(16) into Equation (1c), one can formulate the shear strength by the following equation. Here,  $f'_c$  is considered negative.

$$\tau_{xy}^{max} = \frac{(\sigma_t^{cr} - 0.462f'_c)}{2} \sin 2\theta^{cr} \quad (17)$$

A comparison of experimental data with the predictions by Equation (17) for every unjointed and jointed specimens are shown in Figures 8(a) and (b), along with a  $\pm 10\%$  and  $\pm 20\%$  error ranges. In the case of unjointed specimens, the agreement between the measured and calculated shear strength is indeed good within  $\pm 10\%$  error range. In the case of jointed specimens, the predictions give slightly larger deviation from experimental results than unjointed specimens and are almost within  $\pm 20\%$  error range.

Here, it should be noted that the present formula for shear strength is applicable to the geometric and

loading configurations of the specimens presented in this paper. In order to apply the formula to other configurations, further numerical study may be necessary.

## 5 CONCLUSION

In this paper, an experimental study on plain concrete subjected to shear was carried out. In order to study the shear softening characteristics of plain concrete, a mechanical model for the macroscopic shear failure is applied to the experiment, focusing on the entire load-displacement relation. From this study, the following conclusions can be drawn.

- 1) The analysis employing the proposed mechanical model agrees well with the experimental results on load-displacement curves consisting of the post-peak region. Furthermore, a formula for shear strength is developed and the prediction with the formula is found in good agreement with the experimental data.
- 2) The shear softening characteristics depend on the size of strain localized area. Specifically, the larger width of strain localized area gives the larger post-peak ductility and larger dissipated energy with a slight reduction of the peak stress.

Future work must be directed at further verification studies with experimental observations and alternative analytical studies consisting of several constitutive models in order to generalize the analytical conclusion identified in this paper.

## 6 PREFERENCES

- Balakrishnan, S., & Murray, D. 1988. Concrete Constitutive Model for NLFE Analysis of Structures, *Journal of Structural Engineering*, ASCE, Vol.114(7).
- Bazant, Z.P. & Oh, B.H. 1983. Crack Band Theory for Fracture of Concrete, *Materials and Structures*, RILEM, Vol. 16, pp.155-177.
- Chen, W.F. 1982. *Plasticity in Reinforced Concrete*, McGraw-Hill Book Company.
- Hillerborg, A., Modeer, M. & Petersson, P.E. 1976. Analysis of Crack Formation and Crack Growth in Concrete by Means of Fracture Mechanics and Finite Elements, *Cement and Concrete Research*, Vol.6, No.6, pp.773-782.
- Hillerborg, A. 1985. Numerical Methods to Simulate Softening and Fracture of Concrete in Fracture Mechanics of Concrete: *Structural Application and Numerical Calculation* (ed. Sih, G. C. and DiTommaso, A.), Martinus Nijhoff Publishers, pp. 141-170.
- Hognestad, E. 1951. A Stud of Combined Bending and Axial Load in Reinforced Concrete Members, University of Illinois Engineering Experimental Station, *Bulletin Series* No.399, 128 p., November.
- Hsu, T. T. C., Mau, S. T. & Chen, B. 1987. Theory of Shear Transfer Strength of Reinforced Concrete, *ACI Struct. J.*, Vol. 84, No. 2, Mar.-Apr., pp. 149-160.
- Ishihara, S, Mihashi, H., Kaneko, Y., Mori, K. & Uchii, E. 2003. Experimental Study of Notched Concrete Block Subjected to Shear - Study using Micromechanics Approach -, *Journal of Structural and Construction Engineering*, Architectural Institute of JAPAN (Transactions of AIJ), No. 570, pp.145-150, Aug. (in Japanese).
- Kaneko, Y., et al. 1993a. Fracture Mechanics Approach for the Failure of Concrete Shear Key: Theory, *J. of Engineering Mechanics*, Vol. 119, No. 4, ASCE, pp.681-700, April.
- Kaneko, Y., et al. 1993b. Fracture Mechanics Approach for the Failure of Concrete Shear Key: Verification, *J. of Engineering Mechanics*, Vol. 119, No. 4, ASCE, pp.701-719, April.
- Kaneko, Y. 1993. Fracture Mechanics based Modelling for Failure of Concrete Shear Key and Application to Design of Segmental Structure, *Concrete Research and Technology*, Vol. 4, No. 2, pp.31-41, July (in Japanese).
- Kaneko, Y. 1998. Prediction for Macroscopic Shear Failure of Both Reinforced Concrete Membrane Elements and Reinforced Concrete Deep Beams in terms of Load-Displacement Characteristics, *Concrete Research and Technology*, Vol. 9, No. 2, pp.43-51, July (in Japanese).
- Kaneko, Y., Mihashi, H. & Ishihara, S. 2001. ENTIRE LOAD-DISPLACEMENT CHARACTERISTICS FOR DIRECT SHEAR FAILURE OF CONCRETE, *Modeling of Inelastic Behavior of RC Structures under Seismic Loads*, Committee Report, American Society of Civil Engineers, pp.175-192.
- Kaneko, Y. & Mihashi, H. 2002. Shear Softening Characteristics of Reinforced Concrete Deep Beams, *Journal of Structural and Construction Engineering*, Architectural Institute of JAPAN (Transactions of AIJ), No. 562, pp.115-122, Aug. (in Japanese).
- Mansur, M.A. & Ong, K.C.G. 1991 Behavior of Reinforced Fiber Concrete Deep Beams in Shear, *ACI Struct. J.*, Vol. 88, No. 1, Jan.-Feb., pp. 98-105.
- Rots, J. G. & Blaauwendraad, J. 1989. Crack Models for Concrete: Discrete or Smeared? Fixed, Multi-directional or Rotating ?, *HERON*, Vol. 34, No. 1.
- Soroushian, P., Choi, K. & Alhamad, A. 1986. Dynamic Constitutive Behavior of Concrete, *ACI Journal*, Vol. 83, No. 2, pp. 251-259.
- Vecchio, F.J. & Collins, M.P. 1986. The Modified Compression-field Theory for Reinforced Concrete Elements Subjected to Shear, *ACI Journal*, Vol. 83, No. 2, pp. 219-231.